

[View PDF](#)

Polymer

Volume 54, Issue 1, 8 January 2013, Pages 391-402

Polymer design for high temperature shape memory: Low crosslink density polyimides

Hilmar Koerner, Robert J. Strong, Matthew L. Smith, David H. Wang, Loon-Seng Tan, Kyung Min Lee, Timothy J. White, Richard A. Vaia  

[Show more](#) 

 Outline |  Share  Cite

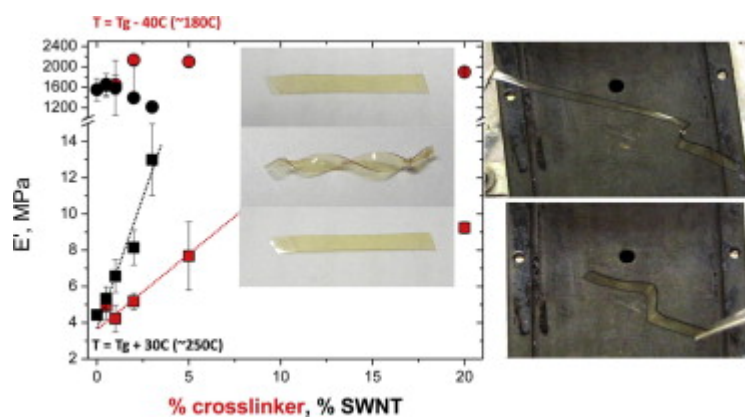
<https://doi.org/10.1016/j.polymer.2012.11.007>[Get rights and content](#)

Abstract

Shape memory in polymers is a process whereby mechanical energy is microscopically stored, and reversibly recovered within the polymer. Consideration of the viscoelastic and glassy dynamics necessary for each step of the process reveals key molecular characteristics that may improve performance, including a rigid polymer backbone with narrow molecular weight distribution between a low fraction of crosslinks. With this insight to guide high temperature polymer design, aromatic CP2 polyimide and associated single wall carbon nanotube (SWNTs) nanocomposites are shown to have excellent shape memory performance at 220 °C with rapid recovery (<10 s), excellent fixity (>98%), good cyclability and outstanding creep resistance. A narrow glass transition temperature regime (<10 °C) and high fragility ($m \sim 117$) affords a narrow triggering window and the ability to spatially localize recovery with a temperature gradient. The addition of up to 3 vol% of dispersed SWNTs improves the rubbery modulus and blocking force without substantially impacting these crucial characteristics. The structure-performance relationships in this material system reinforce the key molecular characteristics for the design of polymers for shape memory.

FEEDBACK 

Graphical abstract



[Download : Download full-size image](#)

[Previous](#)

[Next](#)

Keywords

Shape memory; Polyimide; Nanocomposite

1. Introduction

Shape memory is a process that enables the reversible storage and recovery of mechanical energy through a cyclical change in shape [1], [2]. Currently, commercial shape memory applications use an array of metallic alloys and chemically crosslinked polymers. The application range includes children's toys, intravenous needles that soften in the body, temperature dependent moisture permeable fabrics, rewritable digital storage media and self healing systems [3], [4], [5], [6], [7], [8], [9]. The mechanical energy of deformation is trapped as internal energy and subsequently released with minimal dissipation, by an externally triggered change of the material morphology [10] or a change in the rate of molecular relaxation [11]. To complement the high stress (~500 MPa), but low strain (<10%) performance of metallic alloys [12], crosslinked polymers, and associated micro- and nanocomposites, are being developed for applications demanding light weight and large recoverable strains [13], [14], [15]. These applications include an array of biomedical devices as well as hinges, trusses and booms to move mirrors, unfold reflectors and morph ailerons of aircraft and satellites [16]. Recent reviews summarize the breadth of polymers and composites that are now available for trapping and recovering deformation [17], [18], [19], [20].

FEEDBACK

Surprisingly, two issues are still challenging the broader utilization of many of these high-strain, crosslinked polymeric materials. First is the absence of material systems with operating temperatures in excess of 150 °C. Despite excellent progress toward ambient temperature shape memory, current crosslinked polymers suffer from broad transitions, long recovery times and relatively low triggering temperatures. Although not relevant for most biomedical applications, these higher temperatures are crucial for numerous structural applications in transportation, satellites and aerospace. Also, tooling requirements in automotive and aerospace manufacturing are increasingly demanding narrower triggering temperatures, reduced creep, and accelerated recovery rates – all key limitations when considering polymers or composites thereof. Some notable examples of recent efforts toward these high temperature goals include capacitive CNT mats [21] and electrothermal CNT nanocomposite actuators [22]. However, to maintain deformation with these systems, an external potential must be continuously applied.

The second challenge, which arguably inhibits progress toward the issue considered above, is the absence of a unifying, physics-based framework that enables *a priori* design of polymers at the molecular level for a given shape memory application. Shape memory is not an intrinsic material property, but a characteristic of an engineered system, whether that system is a mechanical design, a composite, or a single material [23]. The term shape memory polymer is commonly used but is misleading in that there is not a special chemical structure or class of polymers that only exhibit shape memory, albeit some are more efficient than others. Prior efforts in constitutive modeling of shape memory have fundamentally adopted the perspective that shape memory is a process [24], [25], [26], [27], [28], [29], [30], [31]. These phenomenological models conceptually divide the polymer into “frozen” and “active” constituents, whose ratio reflects the temperature dependence of viscoelastic relaxation processes. Successful prediction of the shape memory cycle (i.e. deformation-storage-recovery process) is achieved with as many as twelve independently determined parameters. Unfortunately, these models have not allowed extensive investigation of the inverse problem, nor have they provided insight into the molecular level structure critical to optimize performance during any portion of, or across, the shape memory process for environments that are application specific. Thus, the question remains as to what represents the ideal polymer structure for a given shape memory application.

Herein, the deconstruction of shape memory into a series of steps is used to create a framework based on the physics of polymer chain deformation to identify the ideal molecular characteristics of a polymer network for shape memory. With this heuristic insight, aromatic polyimides (PIs) and associated nanocomposites fulfill many of the key characteristics and afford high temperature performance. PIs in general are thermoplastic with a low melt viscosity when prepared via chemical imidization in solution; they are therefore initially impractical for shape memory applications. However, the chains can be controllably crosslinked with a small fraction of triamine. Specifically, lightly crosslinked CP2 (2,2-bis(phthalic anhydride)-1,1,1,3,3,3-hexafluoroisopropane (6FDA) and 1,3-bis(3-aminophenoxy)benzene (APB)) has outstanding thermomechanical properties ($G' \sim 2\text{--}3$ GPa, $T_g \sim 220$ °C) and creep compliance,

glassy dynamics for shape memory, including high fragility ($m \sim 117$) [32], [33] and a narrow glass transition (<10 °C). Furthermore, the addition of up to 3 vol% of dispersed single wall carbon nanotubes (SWNTs) improves the rubbery modulus without substantially impacting these crucial characteristics. The result is a high performance polymer well suited for shape memory applications demanding rapid recovery (<10 s), excellent fixity ($>98\%$), good cyclability and a narrow triggering window at high temperatures. The molecular characteristics revealed by the polymer physics framework are further highlighted by comparing CP2's shape memory performance to other polymer systems.

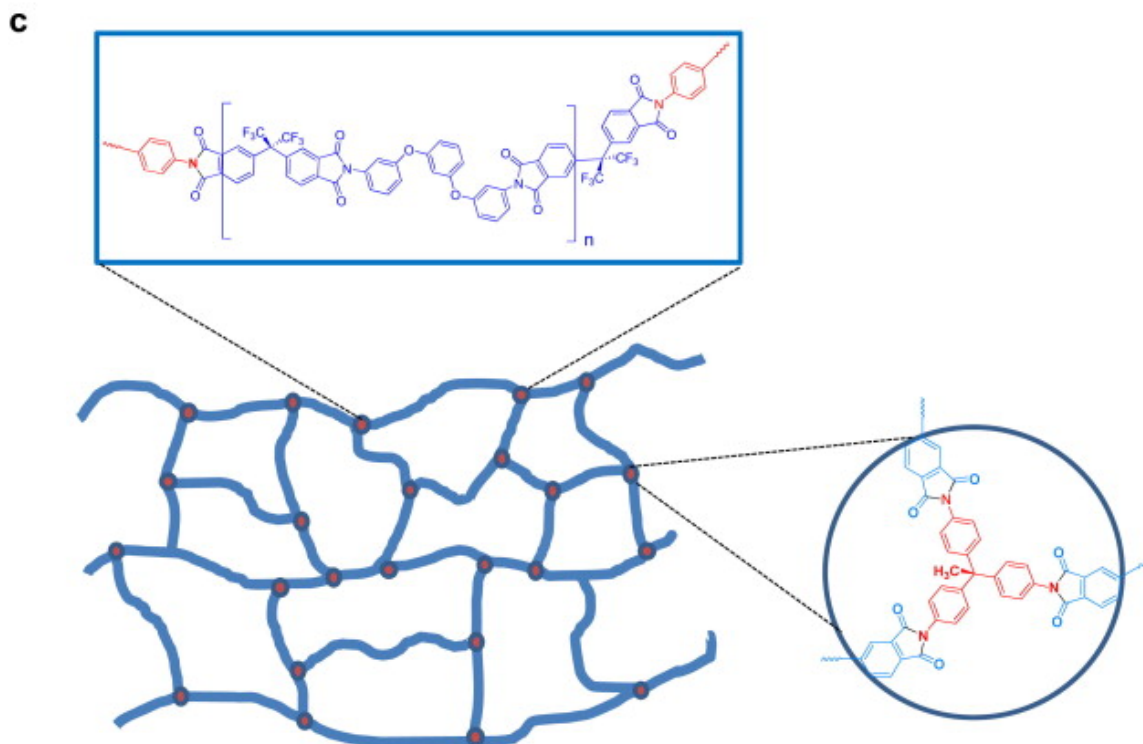
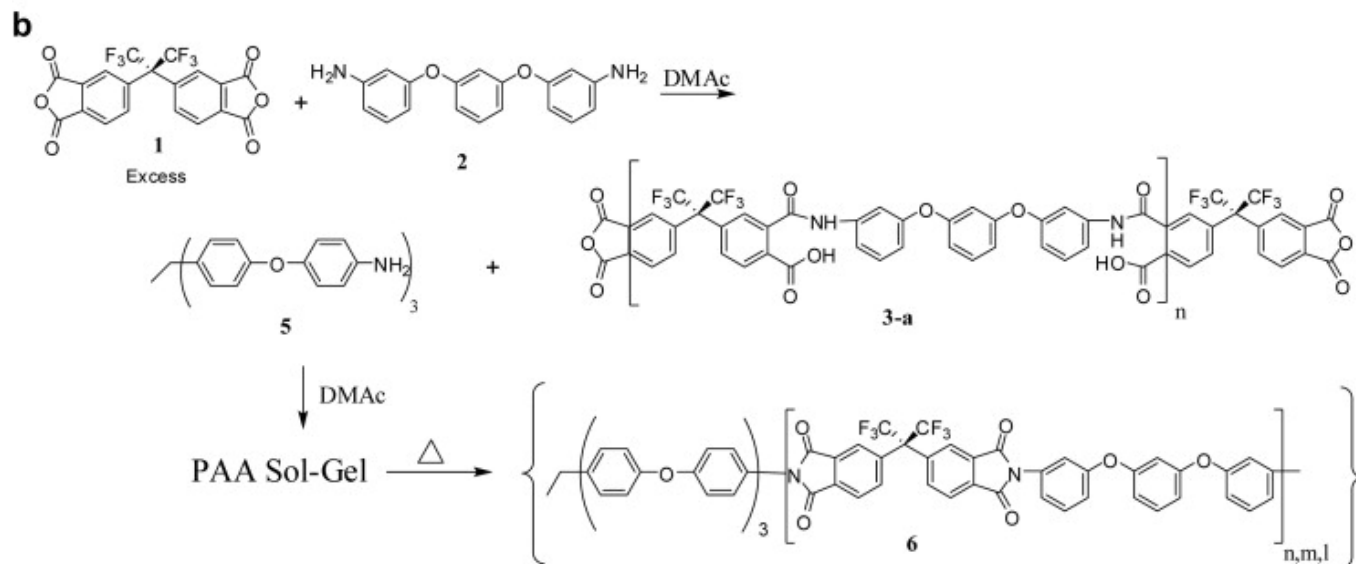
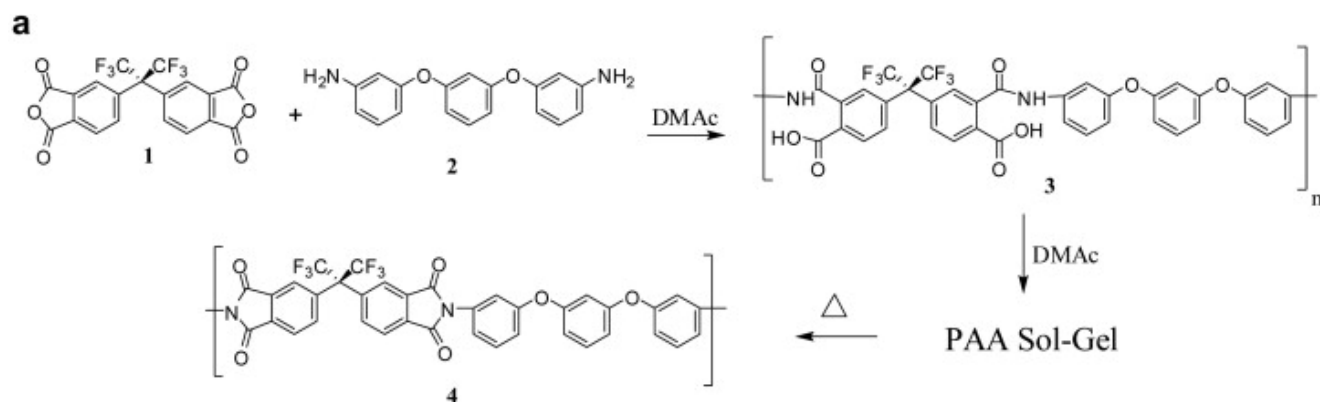
2. Experimental

2.1. Materials

1,3-bis(3-aminophenoxy)benzene (ABP) (99% min.) was purchased from Chriskev Company, Inc. and used as received. Single wall carbon nanotubes (SWNTs) were obtained from LUNA Enterprises, 98.5% pure. All other reagents and solvents were purchased from Aldrich Chemical Inc. and used as received, unless otherwise specified.

2.2. Polymerization

The synthesis of CP2 and crosslinked form were conducted according to previously reported procedures [22], [32] (see Fig. 1). In brief, the diamine **2** (4.0 mmol) and Dimethylacetamide (DMAc) (12 mL) were added to a 50 mL 3-necked flask equipped with a magnetic stirrer, nitrogen inlet and outlet, and stirred under dry nitrogen at room temperature for 30min. 2,2-bis(phthalic anhydride)-1,1,1,3,3,3-hexafluoroisopropane (6FDA) **1** (4.0 mmol) was then charged. The light yellow solution was agitated at room temperature for 24hr to afford a viscous poly(amic acid) (PAA) **3** solution in step **A**. This solution was diluted with DMAc (4–6 mL), poured into a glass dish, followed by vacuum evaporation of DMAc at 50 °C, and heat-treated at: 100 °C/2 h, 150 °C/2 h, 175 °C/1 h, 200 °C/1 h, 250 °C/1 h and 300 °C/1 h to form imidized CP2 **4**. The film thickness was approximately 50–150 μm . Samples with increasing amount of triamine crosslinker **5** were prepared separately in a similar way and by replacing equimolar amounts of diamine with triamine crosslinker (based on functionality ratio) with the additional step **B** (see Fig. 1b, c): triamine crosslinker **5** was added to the anhydride-terminated PAA oligomers **3-a**/DMAc solution, which was first prepared from APB **2** and 6FDA **1** in DMAc in 24 h. After following the curing schedule above, the resulting crosslinked CP2 films **6** are denoted CP2:0.5 for 0.5%, CP2:1 for the 1%, CP2:2 for the 2%, CP2:5 for the 5% and CP2:20 for the 20% according to the mole % of the crosslinker **5** used. Table 1 lists theoretically expected molecular weights based on the molecular weight of a typical neat uncrosslinked CP2 sample (238×10^3 g/mol).



Download : [Download full-size image](#)

FEEDBACK

Fig. 1. Synthesis of (a) CP2 (**4**) polyimides and (b) its crosslink derivatives (**6**) and (c) schematic of crosslinked network resulting from the triamine crosslinker.

Table 1. Physical properties of the CP2 and CP2 nanocomposites.

	Crosslinker mol%/SWNT vol%	MW ^a 10 ³ g/mol	v_e^c 10 ⁵ mol/cm ³	T_g^d °C	Thermal decomposition ^e °C air/nitrogen	G' (50 °C) GPa	G' (T_g-40 °C) GPa	G' (T_g+20 °C) MPa
CP2	0	238		223	521/524	2.1	1.6	4.4
CP2:0.5	0.5	140 ^b	1	222	517/528	2.6	1.7	4.9
CP2:1	1	47 ^b	3	225	519/527	2.5	1.6	4.2
CP2:2	2	24 ^b	6	224	524/525	2.8	2.1	5.2
CP2:5	5	10 ^b	14	226	525/529	2.6	2.1	7.7
CP2:20	20	3 ^b	51	255	520/522	2.4	1.9	9.2
CP2:30	30	2 ^b	71	279	~520	2.4	1.4	13.9
CP2/SWNT:0.5	0.5	239		223	524/527	2.5	1.7	5.3
CP2/SWNT:1	1	371		218	523/528	2.7	1.6	6.6
CP2/SWNT:2	2	136		221	526/530	2.6	1.4	8.1
CP2/SWNT:3	3	136		220	527/531	2.6	1.3	13

a

Molecular weights of CP2 soluble in THF measured by size exclusion liquid chromatography in THF. An average PDI ~ 2.5 was observed.

b

Theoretical molecular weight of chains between crosslinks (M_c).

c

$v_e = \rho_p N / M_c$ where N is Avogadro's number, M_c is average molecular weight of the polymer between crosslinks and ρ_p is the polymer density (1.4 g/cm³) based on swelling studies.

FEEDBACK 

d

T_g was determined from the peak maximum of the DMA $\tan \delta$ curve.

e

Temperature at which 5% weight loss occurred on TGA thermogram obtained with a heating rate of 10 °C/min.

f

FWHM is the full width at half maximum of the $\tan \delta$ peak.

g

Shape memory fixity R_f and recovery R_r , where determined from two cycles ($N = 2$, cycles 2 and 3, average of three specimen per sample) of the shape memory process in extension (SI S6).

CP2 is not a crosslinked polymer when it is prepared in solution from chemical imidization of the poly(amic acid) precursor in a one-pot fashion. As prepared, CP2 is soluble in common solvents such as amide solvents DMAc, DMF and NMP as well as THF and chlorinated solvents. However, in generating film specimens for shape memory experiments, it was more convenient to employ the two-step process with exact monomer stoichiometry that entails casting a poly(amic acid) **3** film on a glass substrate, followed by thermal imidization (cure). In a systematic study of the curing conditions, we found that CP2 films would become insoluble once they were cured above 250 °C, due to covalent crosslinking [34] (details in [Supplemental Information](#)). The resulting crosslink density is reproducible (similar swelling ratio compared to a 0.5% triamine crosslinked sample ($v_e = 1 \times 10^5 \text{ mol/cm}^3$)) and renders CP2 **5** usable in the shape memory process without the need for the triamine crosslinker.

2.3. Nanocomposite formation

Nanocomposite films containing SWNTs were solution cast to an average thickness of approximately 140 μm according to the procedure outlined in prior work [22], [35] with slight modification. In brief, the SWNTs were dispersed homogeneously in anhydrous N,N-dimethylacetamide (DMAc) by sonication. The mixture was shaken using a Mistral Multi-Mixer for 24 h followed by further sonication. Then **1** (6FDA) was added and stirred under dry nitrogen at room temperature until all 6FDA was dissolved followed by the addition of **2** (APB). The dark reaction mixture was agitated at room temperature for 24 h to afford a viscous poly(amic acid) (PAA) **3** solution containing SWNTs in step A. The resulting mixture was diluted with DMAc, agitated for 1 h, sonicated, and poured into a glass dish. DMAc was evaporated under vacuum at 50 °C for 12 h followed by heat treatment at 100 °C/2 h, 150 °C/2 h, 175 °C/1 h, 200 °C/1 h, 250 °C/1 h and 300 °C/1 h under dry nitrogen to convert the PAA to polyimide. Distilled water was added to the casting dish to detach the polyimide film, which was subsequently dried *in vacuo* at 50 °C for 24 h. The polyimide's weight-average molecular weight was 100–200 kDa (according to the results from polystyrene calibrated size exclusion chromatography in tetrahydrofuran (THF)).

25 °C). Note that triamine crosslinker was not added to the SWNT CP2 nanocomposites. Current studies in our group have implied that this is likely due to a dynamic inter- and intrachain crosslinking reaction during polyamic acid forming processes that eventually leads to a small fraction of amide–amide bridges between chains (SI, S1) [34]. As such the triamine crosslinker was not added to the SWNT CP2 nanocomposites. The covalent crosslinking of “neat” CP2 (details in SI, S1), which occurs above 250 °C, provided sufficient network formation to observe shape recovery. Thus all samples examined in this study are crosslinked and insoluble.

2.4. Physical characterization

A strip of polymer (40 mm × 4 mm × 100 μm) was subjected to dynamic mechanical analysis (DMA) at 1 Hz in a nitrogen atmosphere with a heating rate of 4 °C/min on TA Instruments DMA Q800 to obtain temperature dependent storage and loss modulus, transition range and loss factor $\tan \delta$. A standard DMA creep compliance test was carried out by holding a constant stress (2 MPa) on a strip of polymer (40 mm × 4 mm × 100 μm) and monitoring the deformation as a function of time. Transmission XRD (Rigaku Ultrax 18 with Statton camera) and DSC (TA Instruments Q1000 at 10 °C/min) were used to confirm the amorphous character and the glass transition of the polyimide system respectively.

2.5. Shape memory characterization

The shape memory process was evaluated in both tensile and torsional beam geometry. Tensile shape memory was carried out using a modified stress relaxation routine in the DMA (a stress controlled cycle) consisting of 1) heating a sample to $T_g + 20$ °C at 10 °C/min, 2) applying a force that would elongate the sample ~200%, 3) reducing the temperature to $T_g - 40$ °C at 10 °C/min, 4) force removal, 5) heating at 10 °C/min to $T_g + 20$ °C. Once recovery of the sample reached a constant value the cycle was repeated by applying the same force used in step 2). Recovery rates were studied by changing the heating step from $T_g - 40$ °C to $T_g + 20$ °C to a temperature jump. Note that a limitation of the stress controlled TA Instrument DMA Q800 is a finite force that is applied to the sample in the recovery step. Also, temperature ramps in the DMA are limited by heat transfer from medium to polymer due to its inherently low thermal conductivity. This leads to a lag in material response in DMA measurements depending on sample thickness [36]. Further note that due to the narrow transition zone observed in CP2 and derivatives, small deviations in the heating chamber will be amplified by local recovery of the material, such as a non-uniform recovery along the length of the sample and back and front of a sample slab. Therefore to quantify the fast recovery process, determination of the regime where the response was independent of sample geometry as well as a thermal environment more uniform than the DMA furnace was required.

Torsional shape recovery experiments (similar to Rousseau et al. [37]) were carried out in a Squalene oil bath at $T_g + 20$ °C by submerging a twisted strip (40 mm × 4 mm × 50 μm) into the oil and capturing the recovery to the initial flat shape via a portable DinoLite digital

agreement with preliminary results on the surface of a 240 °C hotstage in the ambient, all samples in the torsional recovery experiment recovered in less than a few seconds. The two thermal baths (Squalene oil and ambient air) reduced the convolution of recovery rate and thermal equilibrium of the test equipment (DMA) as noted by previous work on polymers for shape memory [38]. This effective step change in the environment temperature, a large liquid thermal sink, and a large ratio of sample surface area to mass, maximized the rate of thermal equilibrium of the sample. Specifically, experiments were conducted by first twisting a strip of a film a full turn at $T_g + 20$ °C and then locking it in by lowering the temperature below T_g by removal to the ambient. The recovery of the sample after submersion into the high boiling point oil bath (Squalene) at $T_g + 20$ °C was followed via video capture. Video frames of the recovery were analyzed to measure the projected lateral displacement at the midpoint of the ribbon (see SI S2).

Data was analyzed using a viscoelastic beam model under torsion (SI S2) [39], [40], [41], [42], [43]. In brief, modeling the torsional recovery with the viscoelastic beam model under torsion enables quantitative determination of basic material parameters, such as modulus and viscosity, from the recovery rate and time constants. Starting from an extensional Kelvin-Voigt model (Eq. (1)), the torsional recovery of a polymer can be analyzed using analogous equations in shear (Eq. (2)) and solving for the angle of twist φ (Eq. (3)).

$$\sigma(t) = E\varepsilon(t) + \eta \frac{d\varepsilon(t)}{dt} \quad (1)$$

$$\sigma_s(t) = G\gamma(t) + \eta_s \frac{d\gamma(t)}{dt} \quad (2)$$

$$\varphi(\chi, t) = \psi_0 \chi e^{-t/\tau}, \text{ where } \tau = \eta_s / G \quad (3)$$

where χ is the length of the beam, t is time, γ is the shear strain, G is the shear modulus (approximated as 1/3 magnitude of complex extensional modulus $(1/3) \times \sqrt{(G^2 + G'^2)}$), φ is the angle of twist, η is the viscosity (subscript s denotes shear), ψ_0 is the initial rate of twist, τ is the recovery time constant and σ_s is the shear stress. The assumption is made that viscous drag in a liquid medium is very small (viscosity of oil at 250 °C < 1 P) compared to the viscosity of the polymer (>1 kP). The viscosity of the polymer was estimated from values reported in the literature on similar systems, in which the curing reaction was followed until cure cycle completion [44]. Note that Eq. (3) can be extended to include the dependence of recovery rate on sample thickness. It can be demonstrated that with knowledge of basic material parameters such as shear modulus and viscosity, the observed time scale can be predicted as a function of sample thickness (SI S2.2), which allows a direct comparison of recovery times reported in the literature provided material parameters and sample dimensions are reported.

Finally, thermal diffusivity modeling and torsional viscoelastic beam mechanics provides bounds on sample geometry to ensure that observed response is reflective of material characteristics.

Herein the thermal equilibration, and thus the minimum measurable material re

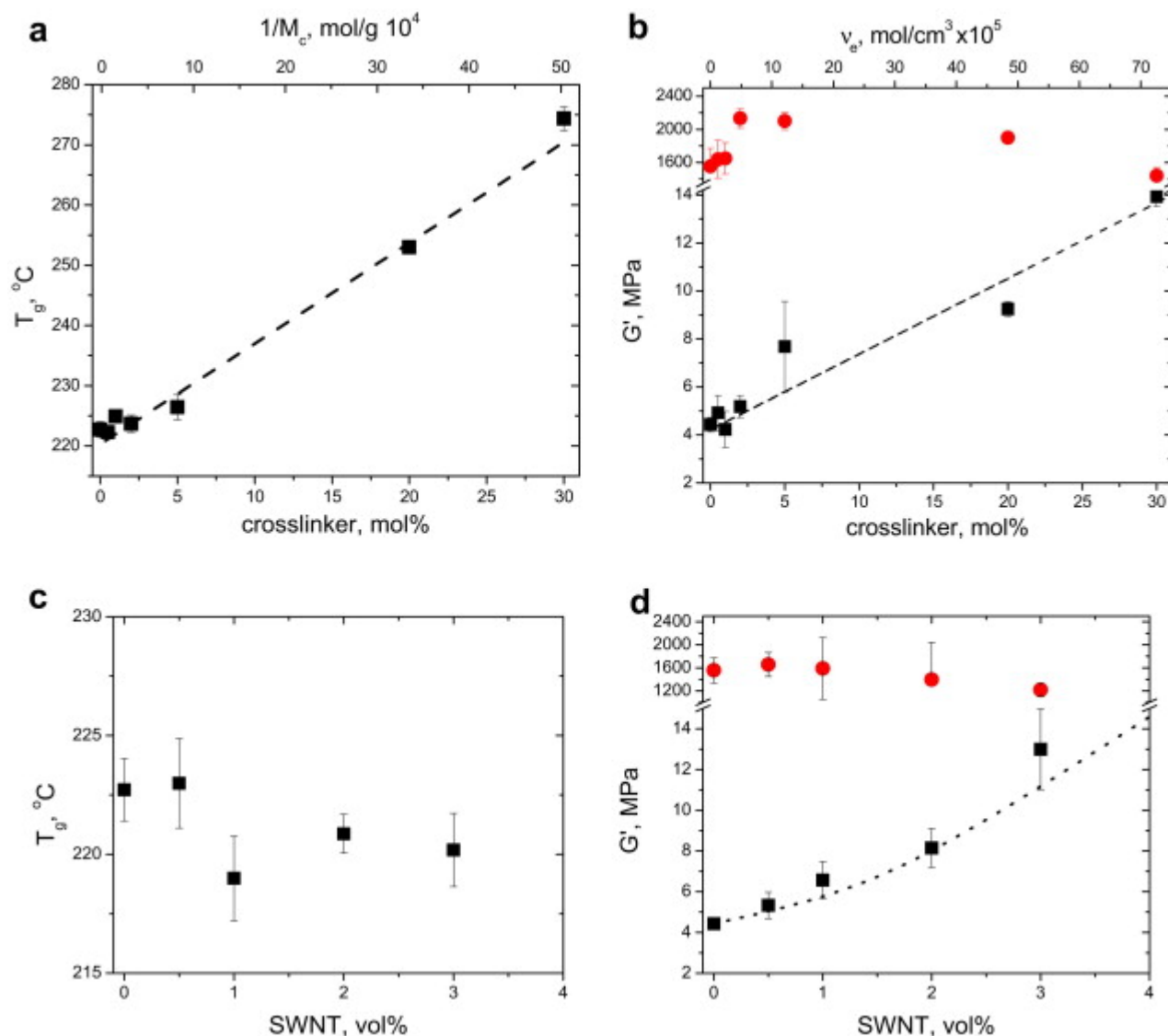
8 ms according to the first term of the solution for thermal transport in a slab [36] ($\hat{T} = (4/\pi) e^{-t/\zeta}$), where \hat{T} is the nondimensional temperature and $\zeta = (4\rho C_p / \kappa \pi^2) b^2$ where we have considered a $40 \times 4 \times 0.05$ mm sample of CP2 (thermal conductivity, $\kappa \sim 0.52$ W/(mK), density, $\rho \sim 1434$ kg/m³, heat capacity, $C_p \sim 1150$ J/(kg K)) experiencing a step temperature change from ambient to 240 °C (or reverse). Likewise, the recovery rate is independent of environment viscosity for twisted slabs greater than 20–30 μ m thick in a medium with viscosities less than 0.12 P (room temperature viscosity of Squalene, SI S2).

3. Results and discussion

3.1. Physical properties of crosslinked CP2

Table 1 summarizes the physical properties of the CP2 systems discussed herein. CP2 is a light yellowish polymer, whose optically clear films are flexible at room temperature. The processing of CP2 films involves the casting of a viscous solution of reacted precursors into a mold and then driving off solvent to start the final curing reaction (see experimental). This enables the design of complex forms that is only limited by the design of the mold. Consistent with prior reports [22], SWNTs are well dispersed in the CP2 as observed by SEM (representative microscopy is included in the **Supplemental information (SI S5)** and conductivity measurements.

Fig. 2 summarizes the glass transition temperature (T_g) and dynamic tensile moduli (G' and G'' at 1 Hz) for the various CP2 and CP2 nanocomposite systems above ($T_g + 20$ °C) and below ($T_g - 40$ °C) T_g . Due to the narrowness of the transition region of these materials, these temperatures are sufficiently removed from the glass transition region to ensure a minimal temperature dependence in moduli, and thus the results can be compared between systems. Complete dynamic mechanical data is provided in SI S3.



[Download : Download full-size image](#)

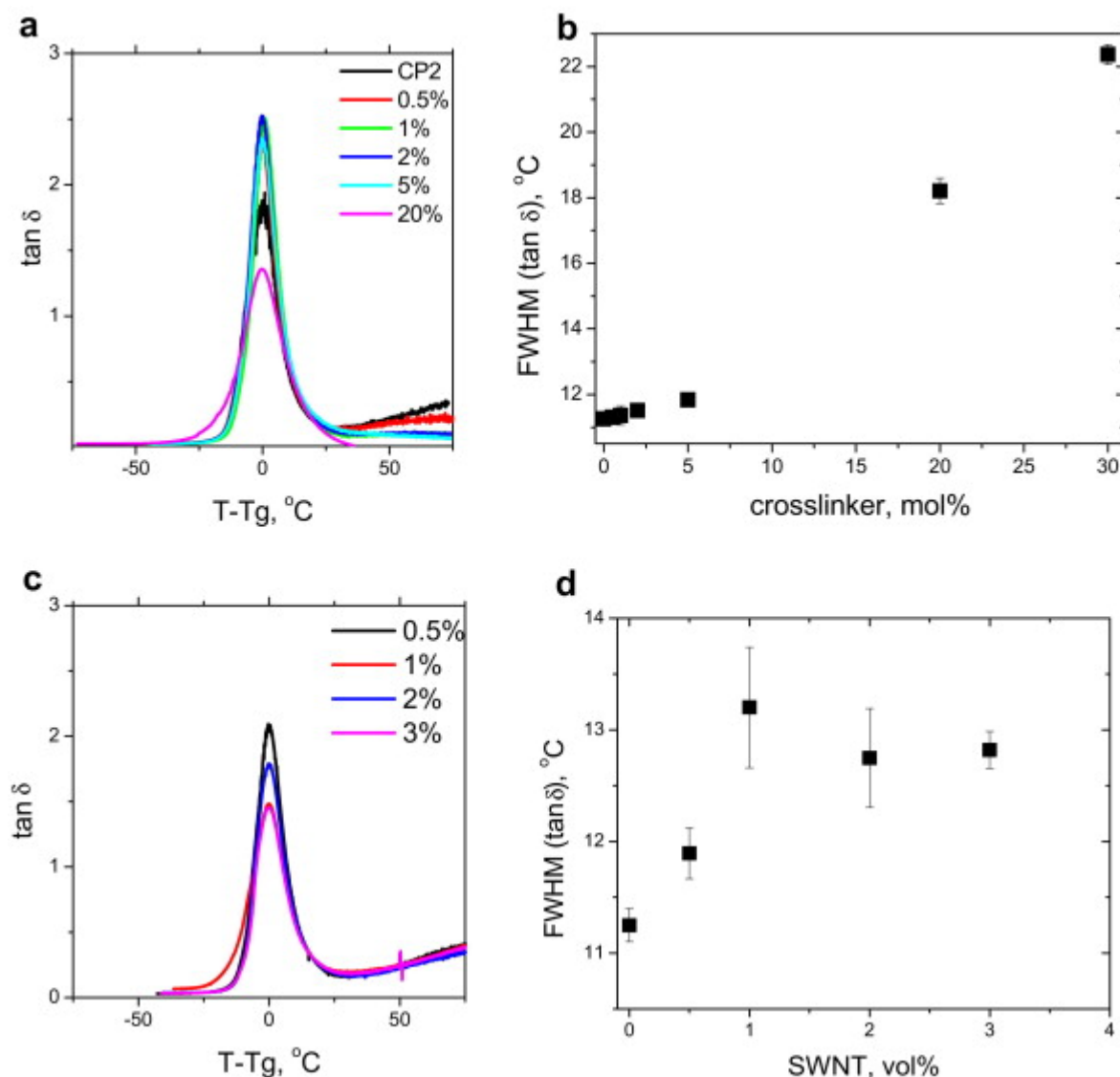
Fig. 2. Summary of glass transition temperatures and moduli of CP2: x and CP2/SWNT: y . a) Temperature of glass transition obtained from $\tan \delta$ peak CP2: x ; dashed line represents linear T_g dependence with $1/M_c$ according to reference [48] ($T_g = T_{g\infty} + \zeta/M_c$, where M_c is the molecular weight between crosslinks, ζ is proportionality factor between molecular weight of unreacted resin and free volume contributions from the resin; and $T_{g\infty}$ is the glass transition of the neat polymer; here $T_{g\infty} = 220.5$ °C, $\zeta = 0.99$ mol/g/K $\times 10^4$). b) storage modulus at $T_g - 40$ °C (red circles) and at $T_g + 20$ °C (black squares) for crosslink series; dashed line represents theoretical prediction from rubber elasticity theory with slope $s = 3RT$. c) temperature of glass transition obtained from $\tan \delta$ peak for CP2/SWNT: y ; d) storage modulus at $T_g - 40$ °C (red circles) and at $T_g + 20$ °C (black squares) for CP2/SWNT: y . Dotted line represents a modulus enhancement according to Guth [55] with an effective particle aspect ratio of 25 [52]. (For interpretation of the references to color in this figure legend, the reader is referred to the web version of this article.)

Table 1 summarizes the crosslinked CP2 films, which are denoted CP2:0.5 for 0.5%, CP2:1 for the 1%, CP2:2 for the 2%, CP2:5 for the 5% and CP2:20 for the 20% according to the mole % of the crosslinker. Neat CP2 exhibits a glass transition of 222 °C (DMA, 1 Hz). The T_g increases approximately linearly with crosslink density (Fig. 2a). About a 5 °C increase is observed for CP2:5, whereas the T_g shifts by 50 °C for CP2:30. This linear relationship is consistent with prior experimental reports of various polymer networks [45], [46], [47]. Additionally, it agrees well with the theory by Banks and Ellis [48] (dashed line Fig. 2a) that relates the change in T_g with the inverse molecular weight between crosslinks, $1/M_c$, based on the addition and redistribution of network free volume. The glassy modulus ($T_g - 40$ °C) of lightly crosslinked CP2 is approximately 1.8 GPa, and increases marginally (~25%) for crosslinking content above 3%. In contrast, rubber moduli increased by almost 100% at 5% crosslinker ($v_e \sim 15 \times 10^5$ mol/cm³). The observed enhancement of the rubbery modulus is directly related to the crosslink density according to the theory of rubber elasticity ($G' = 3vRT$) [49]. The dotted line with a slope of $3RT$ in Fig. 2b demonstrates good agreement between crosslinked CP2 and these theoretical predictions.

Addition of low volume fractions of SWNTs (0.5–3%) to CP2 decreases the glass transition temperature only slightly ($\sim \Delta 3$ °C, Fig. 2c). CP2/SWNT nanocomposites are denoted CP2/SWNT:y with $y = 0.5, 1, 2$ and 3 where y is the volume % of SWNT in the polyimide matrix. Various reports, including Siegel et al. [50] and Pissis et al. [51], report similar impacts on T_g by incorporation of nanofillers into glassy polymers. This slight reduction in T_g is thought to reflect a weak interaction between the filler and interface. In concert, the addition of SWNT increases the rubber modulus. This increase is in quantitative agreement with prior studies that report an increase in the relative moduli, G'/G'_0 of 2.7–3 for ~3 vol% addition (e.g. $G'/G'_0 = 2.9$ for CP2/SWNT:3 and $G'/G'_0 = 2.7$ for Polyurethane/CNT 3 vol%) [52]. Furthermore, the increase in rubbery moduli is consistent with the theory of particulate filled rubbers [53], [54]. Good agreement is observed (dashed line, Fig. 2d) with broader literature trends that were highlighted in previous studies [52] using the Guth [55] model with an anisotropic filler (effective aspect ratio of 25) to describe the average rubbery modulus enhancement. As noted in this prior work, the lower than expected effective aspect ratio (given the large aspect ratio of the primary nanoparticles, e.g. >100 for SWNTs) most likely reflects a combination of non-ideal factors that occur across the general literature reports, including non-uniform dispersion, bending and curvature of the particles, and particle network structures forming above the percolation threshold that lead to inefficient stress coupling and strain field shielding, which result in an “effective aspect ratio” that is less than that of the fundamental particle.

Fig. 3 summarizes the $\tan \delta$ peak and associated full width at half maximum for the various CP2 materials. The area under the loss curve reflects the energy dissipation capabilities of the material [56], [57]. The breadth of $\tan \delta$ is related to the distribution of local collective dynamics, whereas the height reflects the relative viscous and elastic character of the polymer. Outside of the highest crosslink densities, the breadth of the glass transition is only 11–13 °C, which is substantially narrower than reported for many other shape memory thermosets (e.g. 30–40 °C).

30–50 °C for bismaleimides, 15–50 °C for methacrylates) [58], [59], [60], [61], [62], [63], [64], [65]. The narrow transition zone is consistent with a moderate to high fragility index ($m \sim 110$ –120), as determined previously from dielectric spectroscopy [32] and differential calorimetric studies [33]. The linear increase in width of the glass transition with crosslink density, especially at crosslinker content below 5 mol% ($v_e \sim 15 \times 10^5 \text{ mol/cm}^3$), is consistent with results from other crosslinked systems and the theory of rubber elasticity [66], [67], [68], [69], [70], [71]. The increase of the breadth with SWNT addition is also consistent with prior nanocomposite reports. For example silica PMMA nanocomposites [72] and carbon nanotube nanocomposites [73], [74], [75] show both an increase in T_g and breadth of transition, reflecting the broader distribution of local molecular environments.

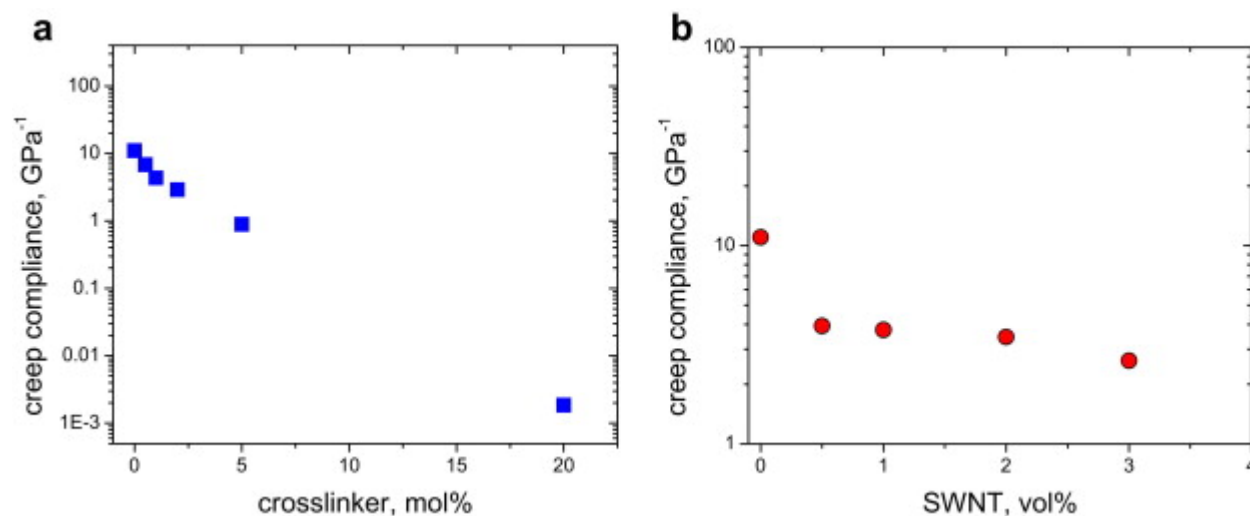


[Download : Download full-size image](#)

Fig. 3. Summary of $\tan \delta$ behavior near T_g of CP2: x and CP2/SWNT: y . CP2: x : a) $\tan \delta$; b) full width at half max (FWHM), ΔT ; CP2/SWNT: y : c) $\tan \delta$; d) FWHM, ΔT .

FEEDBACK

Finally, Fig. 4 summarizes the tensile creep compliance at $T_g - 40$ °C of the CP2 systems under 2 MPa load. Creep is detrimental to the shape memory process, where the temporary shape is under external load. A tendency to creep necessitates fixing of the temporary shape at even lower temperatures, and thus requiring removal of a greater amount of thermal energy. Also, creep behavior restricts the maximum load applied to the temporary shape during application and recovery. For the crosslinked CP2 systems, the creep compliance decreases by over an order of magnitude with incorporation of 5 mol% crosslinker ($v_e = 14.4 \times 10^5$ mol/cm³, CP2:5, Fig. 4a). It reduces by an additional two and a half orders of magnitude for the CP2:20 system ($v_e = 51 \times 10^5$ mol/cm³). For the nanocomposites, the creep compliance decreases by a factor of three with the addition of 0.5 vol% of SWNTs. Further increasing the vol% of SWNTs in CP2 minimally reduces the creep compliance (Fig. 4b). At room temperature, the creep compliance of all the systems was at least an additional three orders of magnitude lower, and less than 10^{-2} GPa⁻¹ (SI S3.2). Overall, the bulkiness of the CP2 monomer increases creep resistance relative to more flexible backbone motifs due to the added stiffness from the conjugated rings [76]. The creep compliance of these systems near T_g ($1-10$ GPa⁻¹) is significantly lower than many other thermoset systems ($10-100$ GPa⁻¹) used in shape memory [77], [78], [79].



[Download : Download full-size image](#)

Fig. 4. Creep compliance at $T_g - 40$ °C of a) CP2: x and b) CP2/SWNT: y . Standard deviation in the creep experiments is 5–10%.

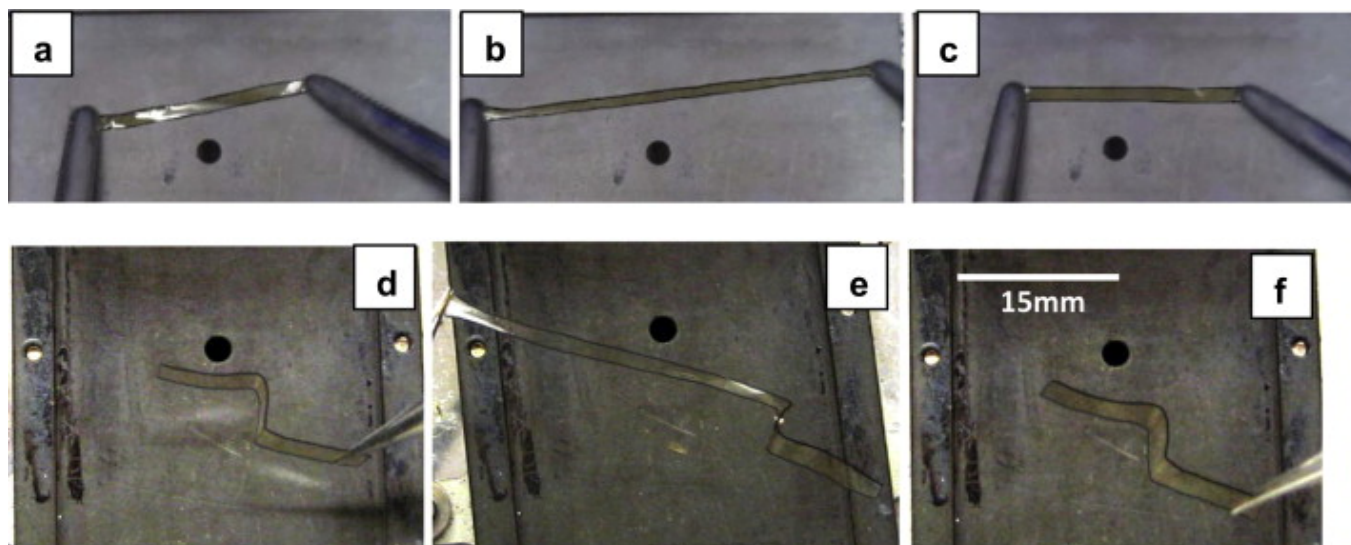
In summary, the thermomechanical properties of the CP2 systems are comparable to prior reports on similar polymer systems. Similar changes in the thermomechanical properties due to crosslinks or nanofiller addition have been reported in other systems [45], [46], [47].

[51], [52], [53], [54], [55], [56], [57], [58], [59], [60], [61], [62], [63], [64], [65], [66], [67], [68], [69], [70], [71], [72], [73], [74], [75], and are in agreement with theoretical models of crosslinked and filled polymer systems. The low to intermediate crosslink density with narrow molecular weight distribution of chains between crosslinks and the rigid backbone on the other hand give CP2 advantage over other thermoset systems at high temperatures.

3.2. Shape memory performance

Two sets of cyclic thermomechanical tests, as outlined in the Experimental section, were used to quantify shape fixity, shape recovery and cyclability [58], [59], [60], [61], [62], [63], [64], [65]. Shape fixity and shape recovery are important engineering assessments of the quality of the entire shape memory process, but depend on both intrinsic characteristics of the polymer and specific details of the process used to observe the shape memory (SI S6). Consistent data necessitates an understanding of the impact of the measurement technique on the thermal equilibration of the sample [36]. For example, the mass and volume of traditional thermal analysis furnaces limit the maximum heating and cooling rates, and challenge the requirement of quasi-uniform sample temperature. Thus the use of numerous techniques is important to ensure material dependent response is separated from external factors.

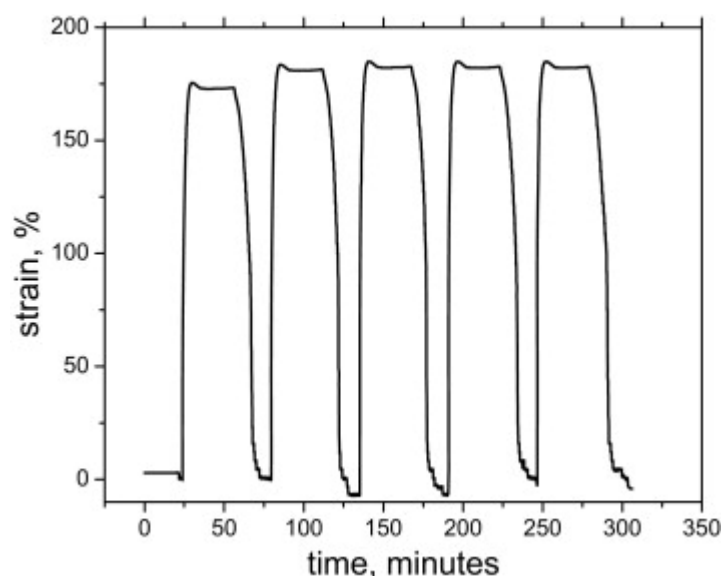
As a representative example, Fig. 5 summarizes the shape memory process for neat CP2. Here the sample ($L_0 = 15$ mm) was heated above T_g on a hotplate ($T_g + 30$ °C) (Fig. 5a), elongated 100% ($\Lambda = L/L_0 = 2$) and fixed by removing the material from the heat source within 1 s (Fig. 5b). Shape fixities were 99–100% (Table 1) for the crosslinked series and 96–99% for the SWNT series. Very rapid (2–5 s) and nearly complete recovery was observed when the sample was returned to the surface of the hotplate ($T_g + 30$ °C) (Fig. 5c). Shape recovery for this cycle ranged from 99 to 100% for the crosslinked samples and 98–100% for the SWNT nanocomposites (Table 1). Overall cyclability was exceptional. After the first cycle, the measured fixities were consistently greater than 99% for the neat CP2. Finally, the shape memory process with CP2 is highly sensitive to temperature gradients. Fig. 5d, e and f show a sample with two independently programmed creases separated by 2 mm, and the subsequent independent recovery of one crease without triggering the recovery of the adjacent crease. No degradation in fixity was observed over 10 cycles and for 5 different crease locations on the sample strip.



[Download : Download full-size image](#)

Fig. 5. CP2 shape recovery process on hotplate at 250 °C. a) original sample, b) stretched sample, c) relaxed sample, d) sample with crease, e) sample with crease elongated adjacent to crease, f) sample with relaxed segment and unperturbed crease. Note, sample edges have been photo enhanced to guide the eye.

The observations (Fig. 5) for neat CP2 were confirmed by cyclic DMA recovery experiments in tension (Fig. 6). Table 1 summarizes values for fixity and recovery observed at $N = 2$ cycles. These values are reproducible up to the examined $N = 10$. The repeatability is excellent (Fig. 6) after at most two work-in cycles. The work-in cycles remove residual stress or slack in the sample mounting resulting from a limitation of the stress controlled DMA system. As crosslink content increases, fixity and recovery values are consistently $>99\%$ (Table 1). Note that CP2:20 and CP2:30 break at elongations $>10\%$ and were not considered in the determination of high-strain fixity and recovery. The addition of SWNTs reduces the fixity and recovery values slightly (96–98%, Table 1). Permanent deformation for these conditions was observed in samples with >2 vol% SWNTs. Reproducibility though, was achievable with a lower maximum strain and a greater number of work-in cycles (3–4) (DMA recovery SI S4).



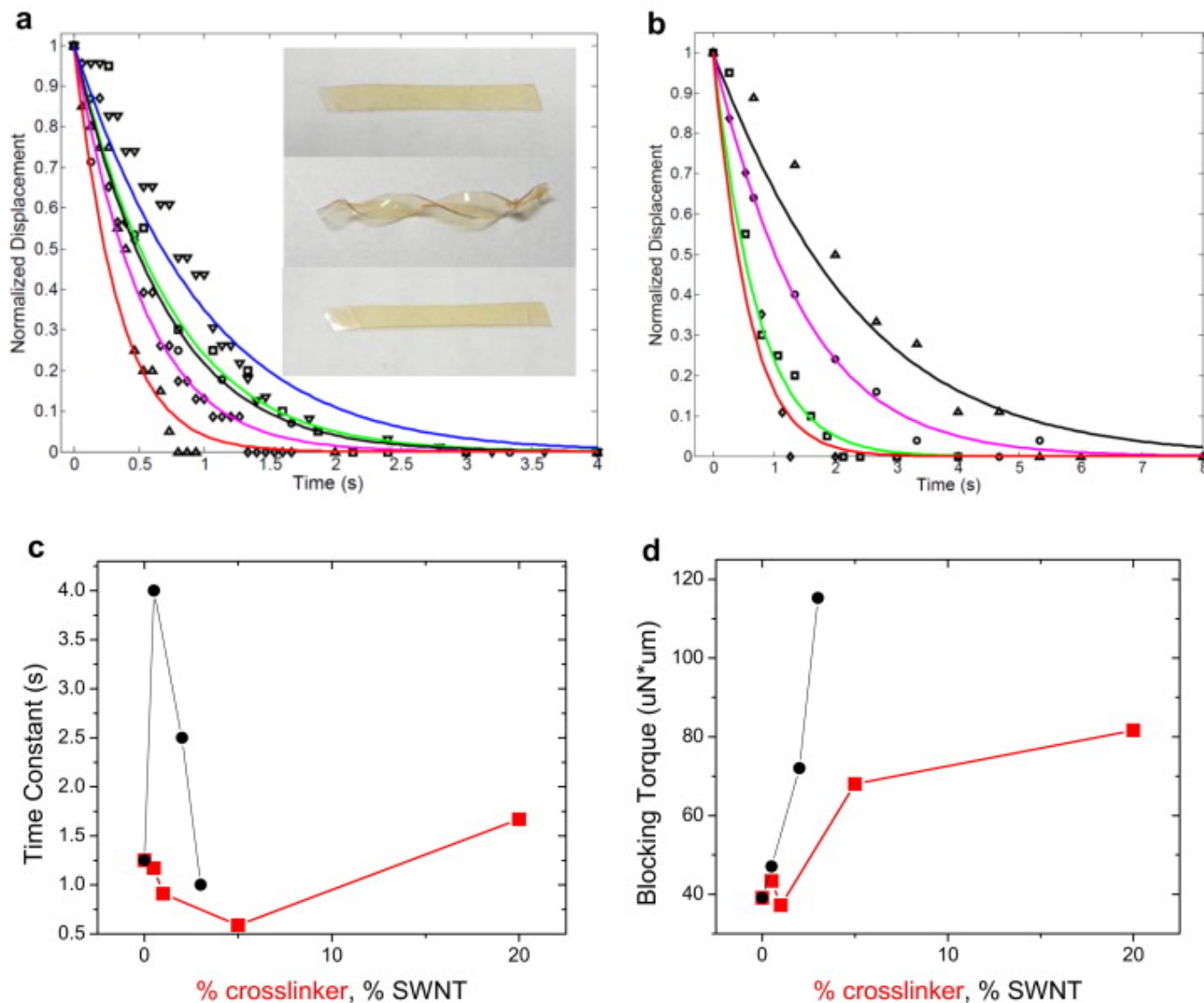
[Download : Download full-size image](#)

Fig. 6. Shape memory cycling in DMA for CP2. A force of 0.1N was applied at $T_g + 10$ °C to deform a sample of 20 mm thickness and 2 mm width to 175%. After a short thermal equilibration (5 min), the sample was cooled (10 °C/min) to $T_g - 40$ °C, the stress released, the sample equilibrated (5 min) and then re-heated (10 °C/min) to $T_g + 10$ °C to trigger recovery.

Temperature jump and relaxation experiments analyzed with torsional viscoelastic beam mechanics provide further quantitative insight into the impact of crosslinking and SWNT content on CP2's utility. With these experiments the recovery time constant τ (approximately the time for 70% recovery in twist with zero external load) and blocking torque, M_{blocking} , can be determined. τ depends on the shear modulus and viscosity of the material. For a fixed geometry and amount of twist, the blocking torque is proportional to the shear modulus (ignoring stress relaxation to obtain a maximum) and represents the maximum amount of work for the given beam geometry that can be accomplished after triggering the shape memory process, where $M_{\text{blocking}} = (1/3)wb^3G2\pi/L$, w is the width, b the thickness, G the shear modulus and L is the length of the sample. Additional details on the temperature jump experiments and analysis are provided in [SI S2](#).

[Fig. 7](#) summarizes the results of the analysis of the torsional shape memory characterization. The temporary shape does not relax upon removal from the temperature bath, yielding a fixity of $\sim 100\%$ that is consistent with that discussed above. The twisted samples retain their shape at room temperature ($t > 9$ months). Most importantly complete recovery of the initial shape occurs after this extended storage, demonstrating no performance loss after long storage times (see [SI, S8.1](#) for details). Upon re-immersion in the temperature bath, time-resolved untwisting of the sample provides a measure of the angle of twist, φ . The projected normalized dist

given by $1 - \cos(\varphi)$, and can be modeled to obtain the recovery time constants (see Eq. (3)). For low crosslink densities, the recovery time constant decreases with increasing crosslink density, implying a faster shape recovery as the network density increases. Between 5 and 20 mol% crosslinker though, the recovery time constant increases. In contrast, the initial addition of a small amount of SWNTs leads to a substantial increase in recovery time constants, which subsequently decreases toward neat CP2 with further additions of SWNTs (Fig. 7c). The observed increase in blocking torque with increasing fraction of crosslinks or nanotubes (Fig. 7d) is expected based on previous results [15] and rubbery modulus data (Fig. 2) for both the crosslink series and the SWNT nanocomposites.



[Download : Download full-size image](#)

Fig. 7. Shape recovery of CP2:x samples at $T_g + 20$ °C. A beam was initially twisted 360° along its long axis in an oil bath at $T_g + 20$ °C, quenched to room temperature, then re-immersed in the oil bath. This results in a maximum shear strain of $\gamma_{\max} = bx2\pi/L = 7.8 \times 10^{-3}$ [80]. a) CP2:x (\square :neat CP2; \circ :CP2:0.5; \diamond :CP2:1; \triangle :CP2:5; ∇ :CP2:20). b) CP2/SWNT:y (\square :neat CP2; \triangle :CP2/SWNT:0.5; \diamond :CP2/SWNT:1; \circ :CP2/SWNT:5; ∇ :CP2/SWNT:20). c) Time constant vs. % crosslinker and % SWNT. d) Blocking torque vs. % crosslinker and % SWNT.

FEEDBACK

○:CP2/SWNT:2; ◇:CP2/SWNT:3) c) recovery time constant determined from fits to the data according to Eq. (3) (■:CP2/x; ●:CP2/SWNT:y). d) blocking torque for every 2π turn (■:CP2/x; ●:CP2/SWNT:y).

3.3. Comparison with available systems

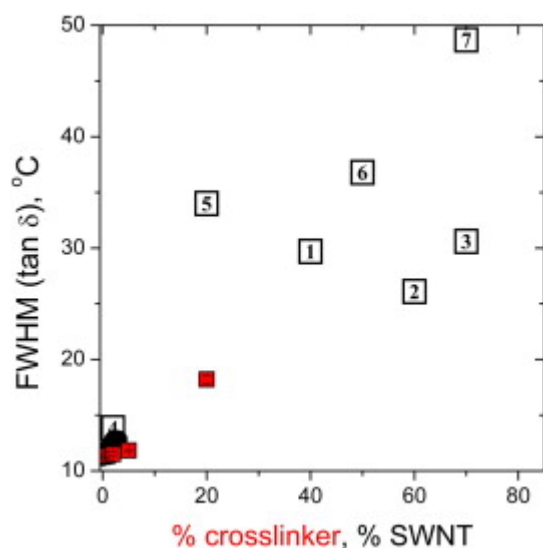
When developing new materials it is instructive to quantitatively compare performance across alternative material systems. Conventionally, thermoset polymers developed for shape memory, such as epoxy based thermosets [59], polystyrene based thermosets [60] and methacrylate based thermosets [63] have relative high crosslink density to ostensibly insure a “memory” of the original shape. Conceptually, the crosslink density is optimized to increase the rubbery modulus at the expense of deformability. However at the molecular level, the structure of highly crosslinked polymer formed by addition or free radical reactions between multifunctional groups are characterized by a random hierarchical network with a large distribution in molecular weight between crosslinks. This spatially non-uniform crosslink distribution results from gelation occurring at reactant conversions of $\sim 50\%$, and subsequent crosslinking being diffusion limited [81]. The probability of network inhomogeneities increases with increasing crosslink density for these chemistries, especially when crosslink densities reach values greater than $50 \times 10^5 \text{ mol/cm}^3$ [66], [67]. The heterogeneities in local environments results in a broadening of the collective spectrum of polymer dynamics, and thus the transition zone. For example, vulcanization studies on rubbers established that the width of $\tan \delta$ generally increases with crosslink densities [68], [69]. Mano et al. [70] and Safranski [71] reported an increase in T_g and in width of $\tan \delta$ with increasing crosslink density in a PMMA system. Asymmetry towards sub T_g temperatures reflect the collective relaxation of regions of the network with less constraints (lower local crosslink density) and higher free volume (more terminal chain ends). These local sub T_g molecular processes are detrimental to the long-term reproducibility and stability of the macroscopic shape memory process. They provide energy dissipation processes far removed from the glass transition. These facilitate stress relaxation and creep, as well as necessitate greater and faster sample cooling for shape fixing, thereby limiting sample thickness and increasing application requirements.

Heuristically, molecular characteristics that impact collective relaxations around a glass transition should directly lead to an understanding of the ideal molecular characteristics for a shape memory process that utilizes a glass transition to retain deformation. A discussion of the underlying polymer physics and the resulting antagonistic relationship for shape memory performance is included in the [Supplemental information \(S7\)](#). In brief, a fragile system with a narrow transition range will ensure the most efficient fixing of a temporary shape. However, a fragile glass inherently has large free volume, which will decrease creep resistance and minimize the maximum load on the material prior to the onset of creep. Alternatively, a network architecture consisting of a narrow distribution of chain lengths between a low d

crosslinks will maximize anelastic deformability in the plateau region for creating the temporary shape. Additionally, it will minimize molecular heterogeneities, and thus narrow the transition region for fixing the shape. However, the plateau modulus will decrease with a decreased crosslink density, reducing the absolute amount of mechanical energy stored and stress recovered for a unit strain. A higher density of random crosslinks intended to increase modulus will decrease the anelasticity and constrain the potential complexity of the temporary shape.

The relative rigidity of the polymer backbone provides an interesting option to balance these requirements, especially for high temperature operation. A rigid polymer backbone should exhibit fragile glass dynamics and a narrow glass transition region as summarized by Sokolov et al. [82]. The rigid nature of the backbone will also afford a degree of stiffness and is synonymous with a high T_g . A low crosslink density with narrow molecular weight distribution will provide large anelastic deformability in the rubbery state while maintaining a narrow T_g regime. In general aromatic polyimides and associated nanocomposites fulfill many of the above characteristics, although condensation polymerization limits the narrowness of the molecular weight distribution. Nevertheless, they are relatively easy to prepare, compared to other high performance polymers, and widely used, ranging from flexible cables, high temperature adhesives, and insulating films for electronics to medical tubing and aerospace structures [83], [84], [85], [86], [87], [88]. Recent demonstrations of efficient methods to trigger recovery using nanocomposites and electrical, microwave, magnetic or optic sources also provide a wealth of facile alternatives to externally imposed sample heating [89].

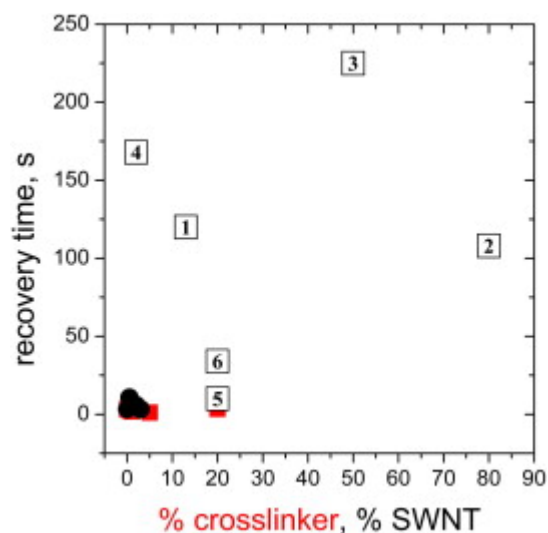
Fig. 8 summarizes the width of the glass transition determined from $\tan \delta$ (DMA) for various polymers used for shape memory. In general the breadth ranges from 25 to 50 °C [58], [59], [60], [61], [62], [63], [64], [65] for systems ranging from epoxies to BMI. CP2 and CP2 nanocomposites achieve the necessary thermomechanical features for shape memory but with a lower crosslink density network that results in a substantially narrower transition region (10–12 °C). Similar narrow transitions for a shape memory process can only be found for epoxy thermosets with long aliphatic Jeffamines with crosslink densities similar to CP2 discussed herein [10]. The glass transition temperature of these systems is close to room temperature however due to the flexible chain segments between crosslinks.



[Download : Download full-size image](#)

Fig. 8. FWHM of $\tan \delta$ at T_g . CP2:x (■); CP2/SWNT:y (●) and available literature data [58], [59], [60], [61], [62], [63], [64], [65] (1–3 [64], 4 [10], 5 [65], 6 [59], 7 [63]).

Fig. 9 compares the recovery times of CP2 (2–5 s) to a set of thermoset systems (50–200 s) with comparably reported recovery times [91], [92], [93], [94], [95], [96], [97]. The limited literature data and spread most likely reflect the issues discussed above where recovery time may depend on sample geometry and test methods due to thermal equilibration limitations. Nonetheless, Fig. 9 does demonstrate the tunability achievable with different polymers, as well as the ability to create faster shape memory processes by considering the chain relaxation processes underlying shape memory.



[Download : Download full-size image](#)

FEEDBACK

Fig. 9. Recovery times for CP2: x (■); CP2/SWNT: y (●) and literature reports (□) [91], [92], [93], [94], [95], [96], [97] (1 [93], 2 [94], 3 [95], 4 [91], 5 [97], 6 [96]).

Along with network structure, the relative flexibility of the backbone and pendant groups also impact dynamics through the glass transition. As noted above, recent work by Sokolov and co-workers [82] established an empirical relationship between molecular structure and fragility, where a rigid backbone or bulky, stiff pendants lead to high fragility. Large values of the fragility index, ($m \geq 100$), are associated with “fragile” glasses where the temperature dependence of collective relaxations deviate substantially from Arrhenius behavior, i.e. decreasing more rapidly with temperature. In contrast, materials with smaller values of m approach Arrhenius behavior through the transition and are termed “strong” glasses. The fragility index for CP2 is 117, which is similar to polypropylene ($m = 122$); and falls between stronger polymer glasses like poly(vinylmethylether) and poly(propylene glycol) (both $m = 75$), and more fragile polymers such as poly(vinyl chloride) and polystyrene ($m = 191$ and 139 , respectively) [32]. The correlation between fragility and chemical structure provides a qualitative guide to help further refine the chemical structure of polymers for shape memory. For example, this implies that even narrower transitions for CP2 could be engineered with the incorporation of bulky pendants in the diamine or dianhydride or replacement of the meta ether linkage in the diamine. Incorporation of rigid backbone units however will necessitate even lower crosslink densities to retain deformability. For example, the theoretical value of degree of polymerization between crosslinks in CP2 with 20% crosslinker is only 3. As summarized by Mark and others, such close crosslinks do not contribute to the elastic deformation of the polymer in the plateau zone [53], [90]. This leads to the rupture of CP2:20 and CP2:30 samples at strains $< 10\%$, while those with lower crosslink density can be stretched $> 200\%$. Overall, these correlations between molecular structure and network dynamics provide a robust framework to introduce the necessary elasticity, thermomechanical properties and transition temperature while minimizing crosslink density ($v_e < 15 \times 10^5 \text{ mol/cm}^3$) and maximizing network uniformity.

In addition to considerations of backbone and network structure, the use of nanofillers provides a tool to optimize steps in the shape memory process. There are many reports demonstrating the value of nanoparticle addition to polymers to provide alternative heating or triggering concepts for shape memory [89]. However, the addition of nanofillers can also be used to increase the rubbery properties of the polymer and thereby increase the energy storage capacity. Numerous reports, ranging from clay to carbon nanotube nanocomposites, concluded that the addition of small amounts of anisotropic inorganic nanofillers efficiently increase rubbery moduli without impairing other mechanical and thermal properties. For example, 3 vol% addition of SWNTs to CP2 increased the plateau modulus by a factor of ~ 3 and thus doubled the blocking torque. This is consistent with previous work that has shown that the energy output in a shape memory

process can be increased by 2–3 times with the addition of small amounts of carbon nanofibers [15], [55].

4. Conclusions

The key criteria for developing a polymer system based on the discrete steps of a shape memory process were laid out with regard to the fundamental characteristics dominating dynamics in a polymer system and its response to an external force. A semi-rigid and bulky backbone, high chain packing density, low crosslink density with uniform crosslink distribution, and high molecular weight between crosslinks provide a balanced approach to these criteria. The low crosslink density CP2 system meets these criteria and exhibits excellent high temperature (220 °C) shape memory performance with fast recovery times (2–5 s), excellent extensibility (>200%), high room temperature modulus (2–3 GPa), outstanding creep resistance, and shape fixity and recovery ratios that are conservatively greater than 98%. The significantly higher glass transition (<220 °C) of CP2, which is due to the comparatively more rigid backbone than BMI or epoxy, affords shape memory temperatures much higher than previously reported. At the same time this higher glass transition affords materials that have little to no creep at room temperature and allow for long periods of storage without performance deterioration. The energy storage, blocking torque, and rubbery modulus can be further increased via the incorporation of SWNTs, which based on prior studies also affords a myriad of multi-functionality including electrical conductivity and potentially electrical, RF and optical control of the shape memory process. In general, the CP2 systems provide a unique solution to numerous applications requiring higher temperature shape memory, such as hinges, trusses and booms to move mirrors, unfold reflectors and morph ailerons of aircraft and satellites, as well as tooling in composite manufacturing.

Although qualitatively successful herein, additional experimental studies are required to refine the proposed correlations between molecular structure, network structure and shape memory performance. Engineering assessments of the shape memory process, such as shape fixity and shape recovery, must be complimented with techniques that directly measure the correlation between material properties and macroscopic behavior in each step. Analogous to energy storage and harvesting devices, measurements of the maximum energy storable, fill factor, and the energy and power efficiency of a set-recovery cycle are necessary to guide network and composite design, determine how close a concept is to ideal behavior and identify the dominant limiting factors. With these refined techniques, material architecture concepts can be quantitatively compared. For example, reversible physical crosslinks, including mesophase separation [98] and polymer crystallites [1], are utilized as an alternative to chemical crosslinks in numerous polymers to define a permanent shape and provide an alternative to a temperature quench to retard recovery of deformed chains. The fundamental steps of the shape memory process are still the same, only the specific material processes to achieve each step are different. In other words, these physical crosslinks create a network topology on the mesoscale analogous to that created by chemical crosslinks on the molecular scale. The correlation between topology, chain structure

relaxation processes should also frame design tradeoffs for optimizing these materials for shape memory processes in different environments. For example as shown with the CP2 systems, high crosslink density is not a prerequisite for high quality shape retention and recovery. Low to intermediate crosslink density provides sufficient elasticity and deformability above T_g , and a high glass transition temperature provides resistance to stress relaxation in the stored shape. Recent reports on photo-defined shape memory may also be cast in this framework [99], [100]. For example, the difference between a photo-elastic and photo-set response of a glassy azobenzene functionalized polyimide depends not only on the chemical details of the network, but also on the crystallinity, physical aging and process by which the azobenzene unit is isomerized between cis and trans forms [101]. These observations all point to the criticality of local free volume, and thus local relaxation processes in mechanical energy storage or elastic recovery. Stepping up to the nanoscale, the synergistic, or independent, impact of the mechanical response of a second interpenetrating phase affords additional questions regarding the coupling between two co-deforming networks. For example, interpenetrating network of nanofillers, such as SWNTs, occur at concentrations above the percolation threshold and result in drastic changes of physical properties, ranging from conductivity to fracture [102]. This second network may also collectively deform in response to external strain, and contribute to energy storage through local particle bending, buckling or junction rotation [103]. These possibilities are analogous to mechanical design of compliant structures, and have previously been realized in carbon-fiber reinforced shape memory composites, where mechanical energy storage occurs within the bent fiber [104]. Common to all these questions is the need to deconstruct the process of mechanical energy storage and recovery into its constituent steps so as to better understand the most relevant structure–property correlations.

In summary, shape memory is a process in which the viscoelastic nature of entangled polymer chains affords means to design materials with optimal characteristics for each step. Thus, behavior that is reminiscent of shape memory is common across different polymer systems. Optimization of the molecular architecture based on molecular criteria that connect structure to the key relaxation processes controlling internal energy storage and recovery will allow for future improvements in the performance of materials and thereby expand the use of shape memory process to applications ranging from aerospace, automotive and medical, to dynamic packaging of deployable flexible electronics, photovoltaics and programmable matter.

Acknowledgments

We thank Tao Xie (GM) for helpful discussions. We thank Marlene Houtz for additional DMA and TGA measurements. Funding for this project was available from the Air Force Office for Scientific Research. M.L.S. contributed to this article while holding a National Research Council Research Associateship Award.

Appendix A. Supplementary data

FEEDBACK 

 [Download : Download Word document \(1MB\)](#)

Supporting information (SI), includes details on crosslink formation in neat CP2, viscoelastic model for recovery in torsional shape memory process, supplemental data from dynamic mechanical analysis and SEM of CP2 nanocomposites.

[Recommended articles](#)

[Citing articles \(75\)](#)

References

- [1] M. Behl, A. Lendlein
Mater Today (Oxford, UK), 10 (4) (2007), pp. 20-28
[Article](#)  [Download PDF](#) [View Record in Scopus](#)
- [2] I.A. Rousseau
Polym Eng Sci, 48 (11) (2008), pp. 2075-2089
[CrossRef](#) [View Record in Scopus](#)
- [3] M. Irie
Shape memory polymers
Cambridge University Press, Cambridge (1998)
[Google Scholar](#)
- [4] A. Lendlein, R. Langer
Science, 296 (2002), pp. 1673-1676
 [Download PDF](#) [View Record in Scopus](#)
- [5] G.J. Monkman
Mechatronics, 10 (2000), pp. 489-498
[Article](#)  [Download PDF](#) [View Record in Scopus](#)
- [6] C. Liu, S.B. Chun, P.T. Mather, L. Zheng, E.H. Haley, E.B. Coughlin
Macromolecules, 35 (2002), pp. 9868-9874
[View Record in Scopus](#)
- [7] H.M. Jeong, B.K. Ahn, B.K. Kim
Eur Polym J, 37 (2001), pp. 2245-2252
[Article](#)  [Download PDF](#) [View Record in Scopus](#)
- [8] F. Li, L. Qi, J. Yang, M. Xu, X. Luo, D. Ma

FEEDBACK 

J Appl Polym Sci, 75 (2000), pp. 68-77

[View Record in Scopus](#)

- [9] H. Tobushi, H. Hara, E. Yamada, S. Hayashi
Smart Mater Struct, 5 (1996), pp. 483-491
[View Record in Scopus](#)
- [10] T. Xie, I.A. Rousseau
Polymer, 8 (2009), pp. 1852-1856
[Article](#)  [Download PDF](#) [View Record in Scopus](#)
- [11] A. Lendlein, S. Kelch
Kirk-Othmer Encycl Chem Technol. (5th ed.), 22 (2006), pp. 355-365
- [12] W.M. Huang, Z. Ding, C.C. Wang, J. Wei, Y. Zhao, H. Purnawali
Mater Today, 13 (2010), pp. 54-61
[Article](#)  [Download PDF](#) [View Record in Scopus](#)
- [13] K.M. Lee, T. Chung, P.T. Mather
PMSE Prep, 96 (2007), pp. 958-959
[View Record in Scopus](#)
- [14] W. Voit, T. Ware, R.R. Dasari, P. Smith, L. Danz, D. Simon, *et al.*
Adv Funct Mater, 20 (2010), pp. 162-171
[CrossRef](#) [View Record in Scopus](#)
- [15] H. Koerner, G. Price, N.A. Pearce, M. Alexander, R.A. Vaia
Nat Mater, 3 (2) (2004), pp. 115-120
[View Record in Scopus](#)
- [16] M. Abdulrahim, H. Garcia, R. Lind
J Aircraft, 42 (2005), pp. 131-137
[CrossRef](#) [View Record in Scopus](#)
- [17] T. Xie
Polymer, 52 (2011), pp. 4985-5000
[Article](#)  [Download PDF](#) [View Record in Scopus](#)
- [18] L. Sun, W.M. Huang, Z. Ding, Y. Zhao, C.C. Wang, H. Purnawali, *et al.*
Mater Des, 33 (2012), pp. 577-640
[Article](#)  [Download PDF](#) [View Record in Scopus](#)
- [19] M. Behl, M.Y. Razzaq, A. Lendlein
Adv Mater, 22 (31) (2010), pp. 3388-3410

[CrossRef](#) [View Record in Scopus](#)

- [20] P.T. Mather, X. Luo, I.A. Rousseau
Annu Rev Mater Res, 39 (2009), pp. 445-471
[CrossRef](#) [View Record in Scopus](#)
- [21] S. Gupta, M. Hughes, A.H. Windle, J. Robertson
Diamond Relat Mater, 13 (4–8) (2004), pp. 1314-1321
[Article](#)  [Download PDF](#) [View Record in Scopus](#)
- [22] A.T. Sellinger, D.H. Wang, L.-S. Tan, R.A. Vaia
Adv Mater, 22 (31) (2010), pp. 3430-3435
[CrossRef](#) [View Record in Scopus](#)
- [23] W. Wagermaier, K. Kratz, M. Heuchel, A. Lendlein
Adv Polym Sci, 226 (2010), pp. 97-145
[View Record in Scopus](#)
- [24] Y.C. Chen, D.C. Lagoudas
J Mech Phys Solids, 56 (5) (2008), pp. 1752-1765
[Article](#)  [Download PDF](#) [View Record in Scopus](#)
- [25] Y.C. Chen, D.C. Lagoudas
J Mech Phys Solids, 56 (5) (2008), pp. 1766-1778
[Article](#)  [Download PDF](#) [View Record in Scopus](#)
- [26] J.R. Lin, L.W. Chen
J Appl Polym Sci, 73 (1999), pp. 1305-1319
[View Record in Scopus](#)
- [27] Y.P. Liu, K. Gall, M.L. Dunn, A.R. Greenberg, J. Diani
Int J Plast, 22 (2006), pp. 279-313
[Article](#)  [Download PDF](#) [View Record in Scopus](#)
- [28] H.J. Qi, T.D. Nguyen, F. Castro, C.M. Yakackia, R.J. Shandas
Mech Phys Solids, 56 (5) (2008), pp. 1730-1751
[Article](#)  [Download PDF](#) [View Record in Scopus](#)
- [29] H. Tobushi, T. Hashimoto, S. Hayashi, E. Yamada
J Intell Mater Syst Struct, 8 (8) (1997), pp. 711-718
[View Record in Scopus](#)
- [30] H. Tobushi, K. Okumura, S. Hayashi, N. Ito
Mech Mater, 33 (10) (2001), pp. 545-554

[Article](#)  [Download PDF](#) [View Record in Scopus](#)

- [31] A. Bhattacharyya, H. Tobushi
Polym Eng Sci, 11 (2000), pp. 2498-2510
[View Record in Scopus](#)
- [32] D.J. Jacobs, M.J. Arlen, D.H. Wang, Z. Ounaies, R. Berry, L.-S. Tan, *et al.*
Polymer, 51 (14) (2010), p. 7
[View Record in Scopus](#)
- [33] H. Koerner
Aging studies of CP2 polyimides
AFRL (2012)
[Google Scholar](#)
- [34] Tan L-S. in preparation.
[Google Scholar](#)
- [35] D.H. Wang, M.J. Arlen, J.-B. Baek, R.A. Vaia, L.-S. Tan
Macromolecules, 40 (2007), p. 6100
[CrossRef](#) [View Record in Scopus](#)
- [36] C. Liu, P.T. Mather
Mater Res Soc Symp (2005)
- [37] J. Diani, C. Frédy, P. Gilormini, Y. Merckel, G. Régnier, I.A. Rousseau
Polym Test, 30 (2011), pp. 335-341
[Article](#)  [Download PDF](#) [View Record in Scopus](#)
- [38] X. Luo, P.T. Mather
Adv Funct Mater, 20 (2010), pp. 2649-2656
[CrossRef](#) [View Record in Scopus](#)
- [39] M.T. Shaw, W.J. MacKnight
Introduction to polymer viscoelasticity
Wiley-Interscience, Hoboken, NJ (2005)
[Google Scholar](#)
- [40] J.M. Gere
Mechanics of materials
Brooks/Cole, Pacific Grove, CA (2001)
[Google Scholar](#)
- [41] K.F. Graff

Wave motion in elastic solids

Dover Publications, New York (1991)

[Google Scholar](#)

[42] S.J. Farlow

Partial differential equations for scientists and engineers

Dover Publications, New York (1993)

[Google Scholar](#)

[43] L.H. Sperling

Introduction to physical polymer science

Wiley-Interscience, New York (2001)

[Google Scholar](#)

[44] Y. Han, X.Z. Fang, X.X. Zuo

Polym Lett, 4 (11) (2010), pp. 712-722

[Download PDF](#)[CrossRef](#)[View Record in Scopus](#)

[45] K. Ueberreiter, G. Kanig

J Chem Phys, 18 (1950), p. 399

[CrossRef](#)[View Record in Scopus](#)

[46] T.G. Fox, S. Loshack

J Polym Sci, 15 (1955), p. 371

[CrossRef](#)

[47] H. Gibbs, E.A. DiMarzio

J Chem Phys, 28 (1958), p. 373

[CrossRef](#)[View Record in Scopus](#)

[48] L. Banks, B. Ellis

Polymer, 23 (1982), p. 1466

[Article](#)[Download PDF](#)[View Record in Scopus](#)

[49] J.D. Ferry

Viscoelastic properties of polymers

John Wiley, New York (1980)

[Google Scholar](#)

[50] B. Ash, L. Schadler, R. Siegel

Mater Lett, 55 (2002), pp. 83-87

[Article](#)[Download PDF](#)[View Record in Scopus](#)

[51] D. Fragiadakis, P. Pissis, L. Bokobza

FEEDBACK

Polymer, 46 (2005), pp. 6001-6008

[Article](#)  [Download PDF](#) [View Record in Scopus](#)

- [52] H. Koerner, R.A. Vaia, W. Liu, M. Alexander, P. Mirau
Polymer, 46 (2005), pp. 4405-4420

[Article](#)  [Download PDF](#) [View Record in Scopus](#)

- [53] J.E. Mark
Physical properties of polymers handbook
Springer Science, New York (2007)
[Google Scholar](#)

- [54] E. Guth, O. Gold
Phys Rev, 53 (1938), p. 322

- [55] E.J. Guth
Appl Phys, 16 (1945), p. 20
[CrossRef](#) [View Record in Scopus](#)

- [56] M.C.O. Chang, D.A. Thomas, L.H. Sperling
J Appl Polym Sci, 34 (1) (1987), pp. 409-422
[CrossRef](#) [View Record in Scopus](#)

- [57] J.J. Fay, D.A. Thomas, L.H. Sperling
J Appl Polym Sci, 43 (9) (1992), pp. 1617-1623

- [58] Y. Liu, C. Han, H. Tan, X. Du
Mater Sci Eng, 527 (10–11) (2010), pp. 2510-2514
[Article](#)  [Download PDF](#) [View Record in Scopus](#)

- [59] K. Gall, M.L. Dunn, Y. Liu, D. Finch, M. Lake, M.A. Munshi
Acta Mater, 50 (20) (2002), pp. 5115-5126
[Article](#)  [Download PDF](#) [View Record in Scopus](#)

- [60] G. Li, W.J. Xu
Mech Phys Solids, 59 (2011), pp. 1231-1250
[Veriflex]
[Article](#)  [Download PDF](#) [View Record in Scopus](#)

- [61] M.A. Di Prima, M. Lesniewski, K. Gall, D.L. McDowell, T. Sanderson, D. Campbell
Smart Mater Struct, 16 (2007), pp. 2330-2340
[TEMBO]
[CrossRef](#) [View Record in Scopus](#)

- [62] Y. Liu, K. Gall, M.L. Dunn, P. McCluskey
Mech Mater, 36 (2004), pp. 929-940
[epoxy from CTD]
[Article](#)  [Download PDF](#) [View Record in Scopus](#)
- [63] J. Worzakowska
J Mater Sci, 44 (15) (2009), pp. 4069-4077
[CrossRef](#) [View Record in Scopus](#)
- [64] A. McClung
BMI thermosets
AFRL (2011)
[Google Scholar](#)
- [65] Y. Liu, C. Han, H. Tan, X. Xingwen Du
Polym Adv Technol, 22 (2011), pp. 2017-2021
[CrossRef](#) [View Record in Scopus](#)
- [66] I. Hamerton
The chemistry and technology of cyanate ester resins
Chapman&Hall, New York (1994)
[Google Scholar](#)
- [67] I. Hamerton
Recent developments in epoxy resins
Rapra Technology, Shawbury, UK (1997)
[Google Scholar](#)
- [68] Y. Wang, M. Tian, L. Zhang, J. Ma
J Appl Polym Sci, 107 (2008), p. 444
[Article](#)  [Download PDF](#) [CrossRef](#) [View Record in Scopus](#)
- [69] F.R. Keller, T. Koch, H. Peterlik, S. Seidler, U. Schubert
J Polym Sci Part B Polym Phys, 45 (2007), p. 2215
- [70] N.M. Alves, J.L. Gómez Ribelles, J.A. Gómez Tejedor, J.F. Mano
Macromolecules, 37 (10) (2004), pp. 3735-3744
[CrossRef](#) [View Record in Scopus](#)
- [71] Safranski DL. Master thesis. Georgia Institute of Technology; 2008.
[Google Scholar](#)
- [72] Priestley RD. Ph. D. dissertation. vol. Ph. D.: Northwestern University; 2008.
[Google Scholar](#)

- [73] B.P. Grady
Carbon nanotube-polymer composites: manufacture, properties, and applications
Wiley, New Jersey (2011)
[Google Scholar](#)
- [74] L. Liu, A.H. Barber, S. Nuriel, H. Wagner
Adv Funct Mater, 15 (2005), pp. 975-980
[CrossRef](#) [View Record in Scopus](#)
- [75] J.-B. Baek, C.B. Lyons, L.-S. Tan
Macromolecules, 37 (22) (2004), pp. 8278-8285
[View Record in Scopus](#)
- [76] J. Mark, K. Ngai, W.W. Graessley, L. Mandelkern, E. Samulski, J. Koenig, *et al.*
Physical properties of polymers
(3rd ed.), Cambridge University Press, New York (2003)
[Google Scholar](#)
- [77] G.C. Papanicolaou, A.G. Xepapadaki, G.D. Tagaris
Compos Struct, 88 (2009), pp. 436-442
[Article](#)  [Download PDF](#) [View Record in Scopus](#)
- [78] T.F. Juliano, M.R. VanLandingham, C.A. Tweedie, K.J. Van Vliet
Exp Mech, 47 (2007), pp. 99-105
[CrossRef](#) [View Record in Scopus](#)
- [79] D. Ratna, J. Karger-Kocsis
Polymer, 52 (4) (2011), pp. 1063-1070
[Article](#)  [Download PDF](#) [View Record in Scopus](#)
- [80] S.P. Timoshenko, J.N. Goodier
Theory of elasticity
McGraw-Hill, New York (1970)
[Google Scholar](#)
- [81] C. Feger, W.J. MacKnight
Macromolecules, 18 (1985), pp. 280-284
[CrossRef](#) [View Record in Scopus](#)
- [82] K. Kunal, C.G. Robertson, S. Pawlus, S.F. Hahn, A.P. Sokolov
Macromolecules, 41 (2008), pp. 7232-7238
[CrossRef](#) [View Record in Scopus](#)
- [83] D. Wilson, H.D. Stenzenberger, P.M. Hergenrother

Polyimides

Chapman and Hall, New York (1990)

[Google Scholar](#)

- [84] P.M. Hergenrother
Recl Trav Chim Pays-Bas, 110 (1991), p. 481
[CrossRef](#) [View Record in Scopus](#)
- [85] P.M. Hergenrother
Polyimides and other high-temperature polymers
Elsevier, New York (1983)
[Google Scholar](#)
- [86] J.P. Critchley, G.J. Knight, W.W. Wright
Heat resistant polymers
Plenum Press, New York (1983)
[Google Scholar](#)
- [87] C.E. Sroog
J Poly Sci Macromol Rev, 11 (1976), p. 161
[CrossRef](#) [View Record in Scopus](#)
- [88] S.Z.D. Cheng, F. Li, E.P. Savitski, F.W. Harris
Trends Polym Sci, 5 (1997), p. 51
[View Record in Scopus](#)
- [89] S.A. Madbouly, A. Lendlein
Adv Polym Sci, 225 (2010), pp. 41-95
[View Record in Scopus](#)
- [90] J.R. Falender, G.S.Y. Yeh, J.E. Mark
JACS, 101 (24) (1979), pp. 7353-7356
[CrossRef](#) [View Record in Scopus](#)
- [91] I.A. Rousseau, T. Xie
J Mater Chem, 20 (2010), pp. 3431-3441
[CrossRef](#) [View Record in Scopus](#)
- [92] K. Nagahama, Y. Ueda, T. Ouchi, Y. Ohya
Biomacromolecules, 10 (2009), pp. 1794-1799
[View Record in Scopus](#)
- [93] H. Liu, S.C. Li, Y. Liu, M. Iqbal
J Appl Polym Sci, 0 (2011), pp. 1-8

[CrossRef](#) [View Record in Scopus](#)

- [94] F. Castro, K.K. Westbrook, J. Hermillir, D.U. Ahn, H.J. Qi
J Eng Mater Technol, 133 (2011), pp. 21-25
[View Record in Scopus](#)
- [95] Y.S. Wong, Z.H. Stachurski, S.S. Venkatraman
Polymer, 52 (2011), pp. 874-880
[uncrosslinked]
[Article](#)  [Download PDF](#) [View Record in Scopus](#)
- [96] Y. Tsai, C.-H. Tai, S.-J. Tsai, F.-J. Tsai
Eur Polym J, 44 (2) (2008), pp. 550-554
[Article](#)  [Download PDF](#) [View Record in Scopus](#)
- [97] L. Xue, S. Dai, Z. Li
Macromolecules, 42 (4) (2009), pp. 964-972
[CrossRef](#) [View Record in Scopus](#)
- [98] I.A. Rousseau, P.T. Mather
J Am Chem Soc, 125 (50) (2003), pp. 15300-15301
[View Record in Scopus](#)
- [99] K.M. Lee, H. Koerner, R.A. Vaia, T.J. Bunning, T.J. White
Soft Matter, 7 (9) (2011), pp. 4318-4324
[CrossRef](#) [View Record in Scopus](#)
- [100] K.M. Lee, M.L. Smith, H. Koerner, N. Tabiryan, R.A. Vaia, T.J. Bunning, *et al.*
Adv Funct Mater, 21 (15) (2011), pp. 2913-2918
[CrossRef](#) [View Record in Scopus](#)
- [101] K.-M. Lee, D.H. Wang, H. Koerner, R.A. Vaia, L.-S. Tan, T.J. White
Angew Chem Int Ed (2012)
- [102] S.H. Park, P.R. Bandaru
Polymer, 51 (2010), pp. 5071-5077
[Article](#)  [Download PDF](#) [View Record in Scopus](#)
- [103] Yakobson BI, Couchman LS. Carbon nanotubes: supramolecular mechanics. Dekker
Encycl Nanosci Nanotechnol:587-601.
[Google Scholar](#)
- [104] C.-S. Zhang, Q.-Q. Ni
Compos Struct, 78 (2) (2007), pp. 153-161

[Article](#)[Download PDF](#)[View Record in Scopus](#)[View Abstract](#)

Published by Elsevier Ltd.

[About ScienceDirect](#)[Remote access](#)[Shopping cart](#)[Advertise](#)[Contact and support](#)[Terms and conditions](#)[Privacy policy](#)

We use cookies to help provide and enhance our service and tailor content and ads. By continuing you agree to the **use of cookies**.

Copyright © 2021 Elsevier B.V. or its licensors or contributors. ScienceDirect® is a registered trademark of Elsevier B.V.

ScienceDirect® is a registered trademark of Elsevier B.V.

[FEEDBACK](#)